Synthesis of Linde type A zeolite–goethite nanocomposite as an adsorbent for cationic and anionic pollutants

Joseph Kugbe*, Naoto Matsue, Teruo Henmi

Laboratory of Applied Chemistry for Environment Industry, Faculty of Agriculture, Ehime University, 3-5-7 Tarumi, Matsuyama 790-8566, Japan

A R T I C L E   I N F O

A B S T R A C T

Linde type A zeolite (LTA)–goethite nanocomposite was synthesized by adding sodium orthosilicate solution to goethite, followed by addition of sodium aluminate and NaOH solutions at 100 °C. Optimum condition at the Si addition step required for nanocomposite formation was pH 10.0 and Si/Fe = 2.7. The final product composed mainly of LTA and goethite crystals. Formation of LTA–goethite nanocomposites in the final product was suggested by differences in IR spectra and SEM images between the final product and a mixture of LTA and goethite. The mixture separated into LTA and goethite components after washing with water, but the final product did not show such separation. Precipitation of silica on the surface of goethite and subsequent formation of Si–O–Fe bonds at the Si addition step contributed to formation of the LTA–goethite nanocomposite. The amount of adsorption of phosphate on the final product was more than 1.6 times the amount adsorbed on the mixture, indicating generation of synergistic effect in the LTA–goethite nanocomposite.

1. Introduction

Various pollution remediation techniques such as adsorption, precipitation, ion exchange and filtration have been employed. Most of these techniques concentrate on removal of only one type of pollutant, which may either be positively charged or negatively charged. Currently, combinations of cation and/or anion exchangers with inorganic cohesion precipitants are generally used for simultaneous removal of both species of pollutants. However, these materials are expensive; and they release huge amounts of counter anions such as Cl^- and $SO_4{}^{2-}$ ions into the treated system [1]. This may require further treatment. There is an increasing need, therefore, to develop adsorbent materials that are not only economically effective at removing both types of pollutants, but that can also be easily synthesized from natural and waste materials [1].

Zeolites, with their permanent negative charges as well as the interconnection of channels and cages that run through their secondary framework structure, are efficient adsorbents for positively charged pollutants such as heavy metals [2]. Zeolites are easily synthesized from industrial wastes such as coal fly ash and paper sludge ash [3,4]. On the other hand, iron minerals such as goethite (α-FeOOH) are common constituents of soils, sediments and aquifers, and are known to be efficient adsorbents for negatively charged pollutants such as phosphates [5]. If zeolite and goethite are mixed, it could be used for the removal of both positive and negatively charged pollutants in the environment. However, a simple mixture of the two components results in separation into zeolite and goethite components in aqueous solutions: hence does not effectively adsorb the two types of pollutants at the same point in time. A nanocomposite of zeolite and goethite, on the other hand, could be used in remediation of environments without the separation problem. In addition, nano-level composition of zeolites with other materials has resulted in tremendous increase in useful characteristics [6–10]. For example, Fukugaichi et al. [6] found that the amount and rate of decomposition of acetaldehyde under UV irradiation was much higher on a nanocomposite of faujasite type zeolite and anatase type TiO_2, than on a mixture of the two components.

Synthesis of zeolite–goethite nanocomposite has not been reported in literature: one reason is that coexisting Si and Al inhibit the formation of goethite [11,12] when zeolite and goethite were simultaneously synthesized. The aim of this study was, therefore, to synthesize stable zeolite–goethite nanocomposites as fundamental study for syntheses of the nanocomposite from natural and waste materials. In the synthesis procedure, silica was first precipitated on the surface of synthesized goethite. An Al source was then added to form Linde type A zeolite (LTA, $NaAlSiO_4$) on the surfaces of goethite crystals to obtain the LTA–goethite nanocomposite. The nanocomposite was not obtained by simultaneous syntheses of LTA and goethite. Neither was it obtained by synthesis of goethite in the presence of LTA. LTA was selected as a zeolite species, because it is readily synthesized from a wide range of Si and Al sources under a wide range of synthetic conditions [13].

---

* Corresponding author. Tel.: +81 89 9469681; fax: +81 89 9774364.
E-mail address: joekugbe@agr.ehime-u.ac.jp (J. Kugbe).

2. Materials and methods

2.1. Synthesis of LTA and goethite

LTA was synthesized according to the procedure recommended by the International Zeolite Association's Synthesis Commission [14]. For a batch synthesis, 40 mL of 0.0378 M sodium aluminate ($Na_2O\cdot Al_2O_3\cdot 3H_2O$) solution in 0.226 M NaOH was quickly added to 40 mL of 0.0731 M sodium metasilicate ($Na_2SiO_3\cdot 5H_2O$) solution in 0.226 M NaOH. Composition of the mixture was 3.17 Na_2O:Al_2O_3:1.93 SiO_2:128H_2O. The mixture in a polyethylene flask was continuously stirred until homogenized and then heated at 100 °C for 4 h under a water-cooled reflux condenser. The content was then washed with water, dried at 40 °C for 24 h, and used as a synthetic LTA.

Goethite was prepared according to the method of Schwertmann and Cornell [15]. For each batch synthesis, 180 mL of 5 M NaOH solution was rapidly added with continuous stirring to 100 mL of 1.0 M $Fe(NO_3)_3\cdot 9H_2O$ solution in a polyethylene flask. The mixture was immediately diluted to 2 L with water, capped, and kept at 40 °C for 3 weeks. The content was then washed with water, dried at 40 °C for 24 h, and used as a synthetic goethite.

2.2. Synthesis of LTA–goethite nanocomposite

2.2.1. Si coating on goethite

To 1 g of the synthetic goethite, different concentrations of sodium orthosilicate (Na_4SiO_4) were added to obtain Si/Fe atomic ratio of 1.0, 2.7, 5.0 or 10. Water was added to the mixture to achieve goethite/water ratio of 1 g/100 mL, and pH of the mixture was adjusted to 10.0, 11.0, 12.0 or 14.0 with HNO_3 or NaOH solutions. The mixture was heated at 100 °C for 24 h in a polyethylene flask with a water-cooled reflux condenser, then the system was cooled to room temperature. The mixture was then washed with water, centrifuged, and then dissolved Si and Fe in the washings were analyzed by means of a polarized Zeeman atomic absorption spectrophotometer (Hitachi, Z-5000). The precipitate was dried at 40 °C for 24 h, and the contents of Si and Fe in the dried precipitate were calculated.

2.2.2. Al treatment

To 0.6 g of the dried precipitate from Section 2.2.1, corresponding concentrations of $Na_2O\cdot Al_2O_3\cdot 3H_2O$ and NaOH solutions were added in polyethylene flasks to obtain Si/Al ratio of 0.963 and Si/Na ratio of 0.304. Water was added to obtain precipitate/water ratio of 1 g/50 mL, and the mixture was aged at 20 °C for 24 h. The mixture was then heated at 100 °C for 24 h under a water-cooled reflux system, and washed with water. The washings were analyzed for Fe, Si and Al by the atomic absorption spectrophotometer as in Section 2.2.1. The precipitate was dried at 40 °C for 24 h, after which its mass was measured. This was used as the final product.

2.3. Adsorption experiments

Water adsorption experiment was carried out by keeping 1 g of sample in an evacuated desiccator at 20 ± 1 °C for 3 weeks, in the presence of a saturated solution of LiCl (relative humidity = 0.15), CH_3COOK (0.20), $CaCl_2$ (0.31), KNO_2 (0.45), $Na_2Cr_2O_7$ (0.52), $NaNO_2$ (0.66), $NaClO_3$ (0.75), $(NH_4)_2SO_4$ (0.81), $ZnSO_4$ (0.90), or $Pb(NO_3)_2$ (0.98). After that, equilibrium mass of each sample was measured. The amount of water adsorbed was calculated from the difference between the equilibrium mass and mass of the sample dried at 105 °C for 24 h.

Lead (Pb) adsorption experiment was carried out by mixing 50 mg of each sample with 30 mL of 0, 2–5 mM $Pb(NO_3)_2$ solutions.

pH of the mixture was maintained at 5.00 ± 0.02 throughout the adsorption experiment. The mixture was shaken at 20 ± 1 °C for 24 h. After centrifugation at 7200 × g for 30 min, Pb concentration of the supernatant was determined by the atomic absorption spectrophotometer as in Section 2.2.1. The amount of Pb adsorbed was calculated from the difference in Pb concentrations before and after the adsorption experiment.

Phosphate adsorption experiment was carried out by mixing 50 mg of each sample with 30 mL of 0–4 mM NaH_2PO_4 solutions. The mixture was shaken at 20 ± 1 °C for 24 h after which equilibrium pH was measured and the mixture centrifuged at 7200 × g for 30 min. Concentration of phosphate in the supernatant was determined by the method of Murphy and Riley [16]. The amount of phosphate adsorbed was calculated from the difference in phosphate concentrations before and after the adsorption experiment.

2.4. Analytical methods for products characterization

Powder X-ray diffraction (XRD) analyses were performed by a Rigaku Miniflex X-ray diffractometer with Cu-Kα radiation generated at 30 kV and 10 mA, between 4–45° of 2θ angles with a step interval of 0.01° and a scanning rate of 1° min^{-1}. Fourier transformed infrared (FT-IR) spectra were measured with a Shimadzu FTIR-8300 spectrophotometer with a spectral resolution of 2 cm^{-1}, where 1 mg of air-dried sample was mixed with 200 mg of oven-dried spectroscopic grade of KBr to obtain a KBr disc. Scanning electron microscopy (SEM) images were obtained by a Hitachi High Technology S-800 electron microscope at an accelerating voltage of 20 kV.

3. Results and discussion

3.1. Characterization of final product

XRD analyses suggested that composition of final product in the LTA–goethite nanocomposite synthesis was strongly affected by pH and Si/Fe ratio at the first Si coating step, where Si was coated on goethite (Section 2.2.1). In order to know the effect of pH on composition of the final product, the pH was first varied at constant Si/Fe ratio of 2.7. The final products at pH of 12.0 and 14.0 gave no XRD peak due to crystalline materials other than goethite. The final products at pH of 10.0 and 11.0 gave peaks of LTA zeolite in addition to those of goethite. But, intensities of peaks of LTA in the final products obtained at pH of 10.0 were much greater than those obtained in the final product at pH of 11.0. Next, the Si/Fe ratio was varied at a constant pH of 10.0. XRD pattern of final product at Si/Fe of 1.0 was similar to that of goethite, and no peak due to zeolite species was found. The final products at the Si/Fe ratio of 2.7 and 5.0 gave XRD peaks of LTA together with peaks of goethite. Intensity of peaks of LTA was, however, greater for the final product at Si/Fe ratio of 2.7. In XRD pattern of final products at Si/Fe ratio of 10.0, peaks of LTA was not found. We therefore concluded that optimum condition at the first Si coating step was pH 10.0 and Si/Fe = 2.7. Hereafter, the final product obtained at this optimum condition is referred to as "nanocomposite sample".

Fig. 1 shows XRD pattern of the nanocomposite sample, together with patterns of synthetic LTA and synthetic goethite. Lattice parameters of the synthetic LTA and the synthetic goethite agreed well with those for phase identification of LTA (JCPDS number 43-142) and goethite (JCPDS number 29-713). In the XRD pattern of the nanocomposite sample, all peaks were attributed to those of LTA and goethite. The goethite crystallite size distribution ranged from 20 to 50 Å while LTA zeolite crystallite size distribution ranged from 2 to 95 Å. Position and relative intensity of peaks due to LTA
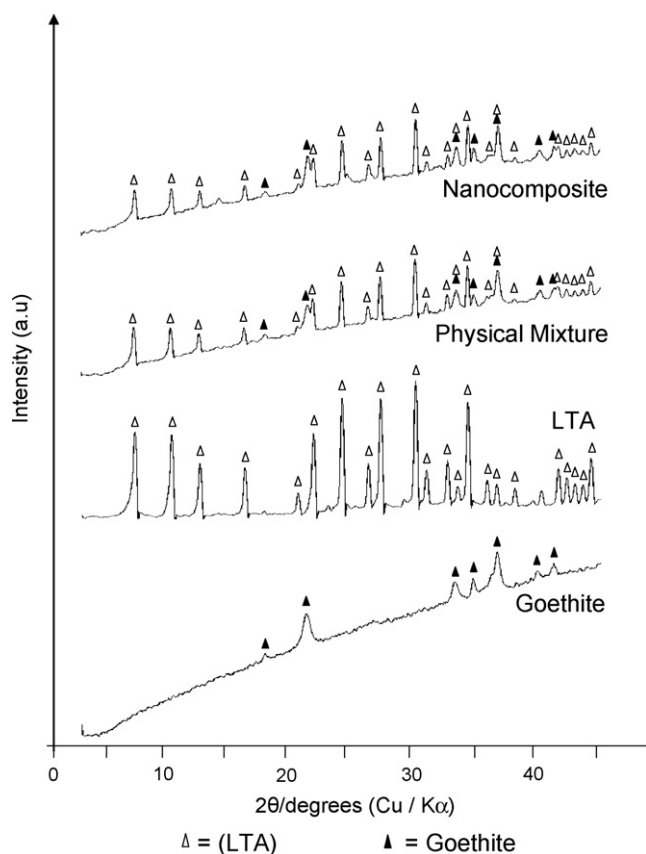
Fig. 1. XRD patterns of nanocomposite sample, LTA–goethite mixture, synthetic LTA and synthetic goethite.

Fig. 2. FT-IR spectra of nanocomposite sample, LTA–goethite mixture, synthetic LTA and synthetic goethite with (a) wider and (b) narrower wave number ranges.

in the XRD pattern of the nanocomposite sample were the same as those in the XRD pattern of the synthetic LTA, indicating chemical structure of LTA in the nanocomposite sample was the same as that of the synthetic LTA. Position and relative intensity of peaks due to goethite in the XRD pattern of the nanocomposite sample were also the same as those in the XRD pattern of the synthetic goethite. A broad peak around 30° was not recognized, indicating amount of amorphous materials composed of Si and/or Al was small in the nanocomposite sample.

Measured mass of the nanocomposite sample was 2.63 g when 1.00 g of goethite was used. Mass ratio of goethite in the nanocomposite sample calculated from the mass determination was 38%, because dissolution of Fe from goethite was negligible throughout the nanocomposite synthesis process (less than 0.2%). Mass ratio of LTA in the nanocomposite sample was then calculated as 62%, by assuming no amorphous materials of Si and/or Al was contained in the nanocomposite sample. Analyses of Si and Al in the washings in Section 2.2 indicated that 39% of Si and 94% of Al of the added materials precipitated as the nanocomposite sample. The Si/Al ratio of LTA in the nanocomposite sample was then calculated as 1.05. Si/Al ratio of pure LTA synthesized in Section 2.1 was calculated as 1.01, by assuming that no amorphous material of Si and/or Al was formed in the synthesis. Both Si/Al ratio values are within previously-reported range of about one for LTA [17].

Fig. 1 also shows XRD pattern of an LTA–goethite mixture. The mixture was obtained by mixing LTA and goethite in water, followed by ultrasonication at 28 kHz for 30 min: mass ratio of LTA and goethite were 62% and 38%, respectively. The XRD patterns of the LTA–goethite mixture and the nanocomposite sample were similar. Intensity of peaks of LTA was, however, a little bit smaller for
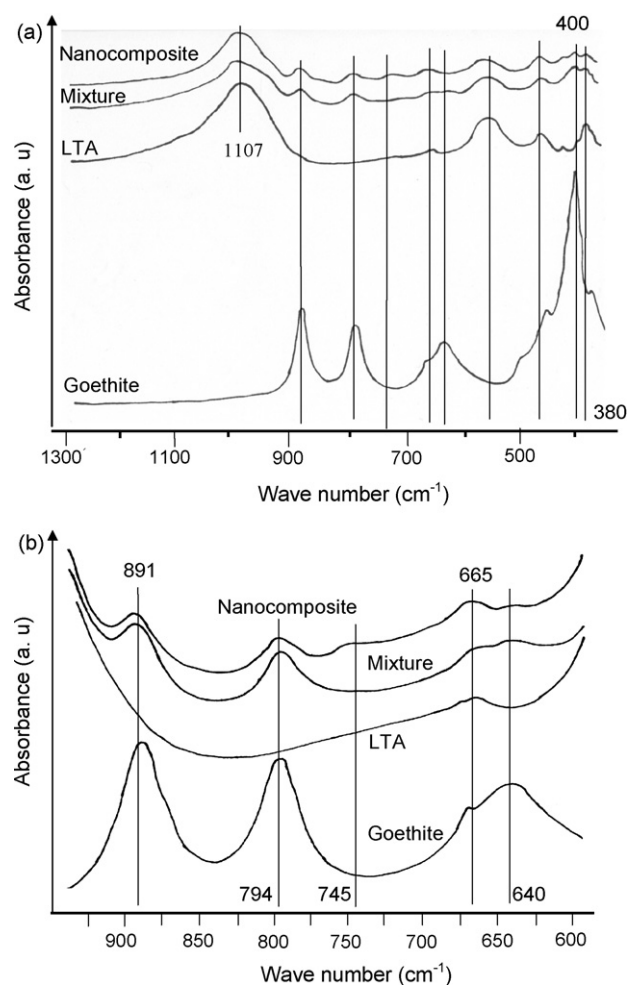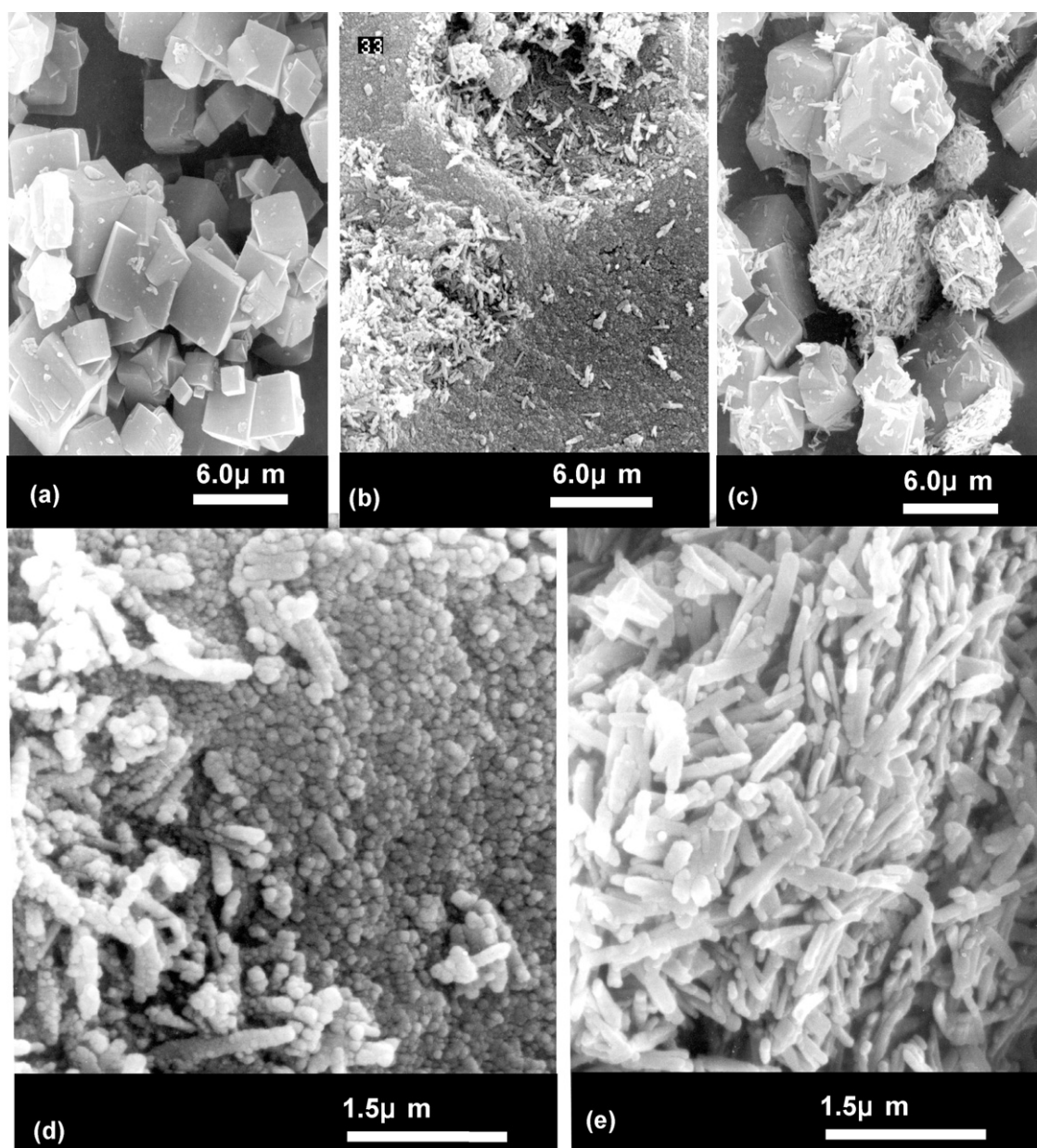
the nanocomposite sample than for the LTA–goethite mixture. This indicates that small amounts of amorphous materials composed of Si and/or Al may have been contained in the nanocomposite sample. However, XRD analyses revealed absence of such amorphous materials.

Fig. 2 shows FT-IR spectra of the nanocomposite sample and the LTA–goethite mixture, together with those of synthetic LTA and goethite, with wider (Fig. 2a) and narrower (Fig. 2b) wave number ranges. A peak at $745\,cm^{-1}$ was found in the spectrum of the nanocomposite sample, but was not found for the LTA–goethite mixture: this peak was also not found for synthetic LTA and goethite. This peak was suspected to be the result of close approach and interaction between LTA and goethite crystals in the nanocomposite sample. Another difference in the spectra between the nanocomposite sample and the LTA–goethite mixture is relative peak height of LTA and goethite. In the spectrum of the nanocomposite sample, intensity of a peak at $640\,cm^{-1}$ due to goethite was much lower than that at $665\,cm^{-1}$ due to LTA, whereas for the LTA–goethite mixture, intensity of the two peaks was comparable. Similarly, in the spectrum of the nanocomposite sample, absorbance of a band at $400\,cm^{-1}$ due to goethite was lower than that at $380\,cm^{-1}$ due to LTA, whereas for the LTA–goethite mixture, band absorbance at $400\,cm^{-1}$ was higher than that at $380\,cm^{-1}$. As described in the previous paragraph, LTA content of the nanocomposite sample was a little bit lower than that of the mixture, while goethite content in the two samples were the same. Therefore the lower relative

Fig. 3. SEM images. Low magnification images of (a) synthetic LTA, (b) nanocomposite sample and (c) LTA–goethite mixture: high magnification images of (d) nanocomposite sample and (e) LTA–goethite mixture.

intensity of peaks of goethite in the nanocomposite sample, as compared to that in the LTA–goethite mixture, indicates incorporation of goethite into LTA body, or covering of goethite by LTA in the nanocomposite sample.

Fig. 3 shows SEM images of the nanocomposite sample and the LTA–goethite mixture. In both samples, long acicular, needle-like goethite crystals were found with multidomain structure along their needle axis (Fig. 3b and c). The acicular goethite crystals formed aggregations in the LTA–goethite mixture (Fig. 3c), but they appeared to be arranged in an order on the surface of LTA crystals in the nanocomposite sample (Fig. 3b). Higher magnification images showed two types of arrangements of goethite and LTA in close proximity. The goethite crystals in the LTA–goethite mixture appeared to be held with their acicular ends stacked on the LTA crystal to form the regularity in their surface arrangement on the LTA crystal (Fig. 3e). On the other hand, formation of finer LTA crystals on the surfaces of goethite crystals was noticed in the

nanocomposite sample (Fig. 3d): leading to the formation of undulations, on goethite crystal surfaces, which were not observed in the LTA–goethite mixture (Fig. 3e). The SEM observations together with the FT-IR results indicate that LTA and goethite particles in the nanocomposite sample were closely attached to each other to form LTA–goethite nanocomposites. As a result, after shaking treatment with water, the nanocomposite sample did not separate into LTA and goethite components, but the LTA–goethite mixture separated easily into the two components.
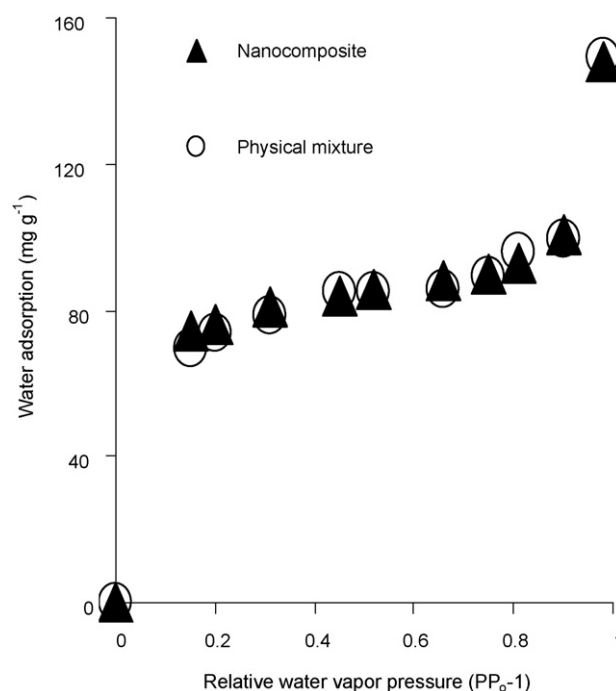
3.2. Mechanism of nanocomposite formation

To clarify the LTA–goethite nanocomposite formation mechanism, chemical state of Si after the first Si coating step was examined by FT-IR spectroscopy. Fig. 4a shows FT-IR spectrum of the sample just after the first Si coating step at the optimum conditions (pH 10.0, Si/Fe = 2.7). The spectrum was compared with that
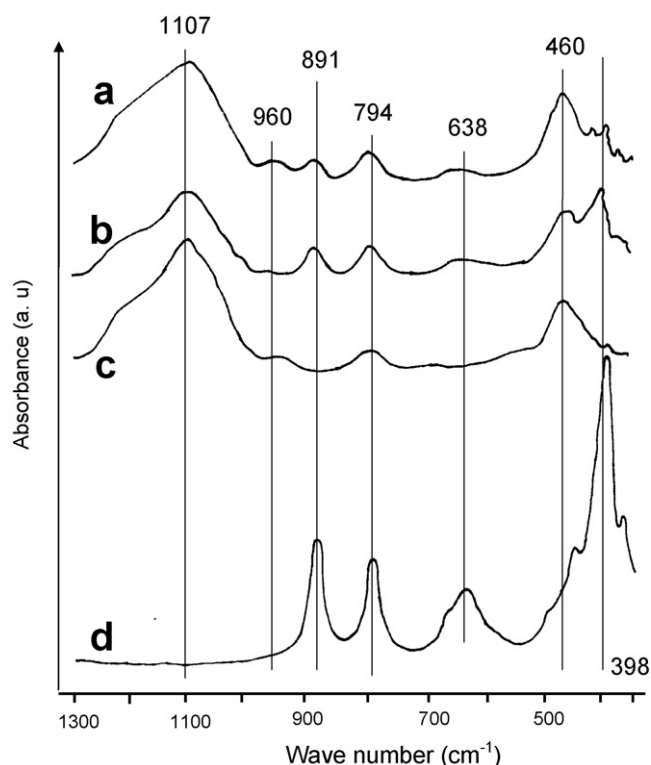
Fig. 4. FT-IR spectra of (a) sample after Si treatment of synthetic goethite at optimum condition (pH 10.0, Si/Fe = 2.7), (b) mixture of synthetic goethite and synthetic silica, (c) synthetic silica and (d) synthetic goethite. The silica was synthesized from sodium orthosilicate by heating at 100 °C for 24 h at pH 10.

Fig. 5. Water vapor adsorption isotherms of nanocomposite sample and LTA–goethite mixture.

of a mixture of silica and synthetic goethite: because the sample at this stage was composed of precipitated silica and synthetic goethite. The silica sample was synthesized by the same method in Section 2.2.1 at Si/Fe = 2.7 and pH 10.0, but in the absence of synthetic goethite. The obtained silica was then mixed and ground with synthetic goethite in a porcelain mortar for 10 min, and used as mixture of silica and goethite: mass ratio of silica and synthetic goethite of the mixture was the same as that of the sample after the Si coating step at optimum conditions (58.7% silica and 41.3% goethite). Fig. 4 also shows FT-IR spectrum of the synthetic goethite: the band at 891 cm^{-1} is attributed to OH deformation vibration in the mirror plane and that at 794 cm^{-1} is to OH deformation vibration out of the mirror plane of goethite [18]. They are considered to be characteristic vibrations in distinguishing goethite [19,20] together with the lattice bands at around 640 and 400 cm^{-1} [19].

FT-IR spectrum of the mixture was just the sum of those of the silica and the synthetic goethite, and no new peak was identified. The spectrum of the nanocomposite sample was qualitatively similar to that of the physically mixed sample; confirming the sample at this stage to be composed of precipitated silica and synthetic goethite. However, relative intensity of the band around 960 cm^{-1} as compared to that at 891 and 794 cm^{-1} (goethite) was higher for the sample than for the mixture. The band around 960 cm^{-1} is related to formation of Si–O–Fe bonds [21–23], indicating that the goethite and silica components in the sample were more closely attached to form Si–O–Fe bonds than those in the mixture of goethite and silica. The band at 960 cm^{-1} also existed in the spectrum of silica (Fig. 4c), but relative intensity of this band compared to that around 1107 cm^{-1} was greater for the sample than for silica. Relative peak intensity of bands of goethite (891, 794, 640 and 398 cm^{-1}) as compared to bands of silica (1107 and 460 cm^{-1}) were

weaker for the sample than for the mixture: this may be due to the covering effect of goethite by silica in the sample.

The mechanism of LTA–goethite nanocomposite formation appears to have involved the adsorption and bonding of Si onto surfaces of goethite; together with precipitation and polymerization of Si, during the Si coating step, onto synthetic goethite. Subsequent Al treatment caused substitution of trivalent Al for tetravalent Si in its tetrahedral framework and rearrangement of Al and Si tetrahedra to form regular lattice of LTA crystals on the surfaces of synthetic goethite, resulting in formation of the LTA–goethite nanocomposite.

3.3. Adsorptive properties of the nanocomposite

Merit for synthesis of LTA–goethite nanocomposite is to generate synergistic properties as an adsorbent for pollutants in addition to solving the separation problem which occurs in LTA–goethite mixtures. Adsorption experiments of water, Pb and phosphate were therefore carried out to examine whether synergistic properties were generated in the nanocomposite sample as compared to the LTA–goethite mixture.

Fig. 5 shows adsorption isotherms for water adsorption by the nanocomposite sample and the LTA–goethite mixture. The isotherm for the nanocomposite sample was similar to that for the LTA–goethite mixture. BET specific surface area of each sample was calculated from the data within monolayer adsorption region of relative humidities between 0.15 and 0.45. Calculated specific surface areas were 157 m^2 g^{-1} for the nanocomposite sample and 160 m^2 g^{-1} for the LTA–goethite mixture: similar values for both samples indicates that synergistic effect was not generated in the nanocomposite sample in view of the specific surface area and water adsorption. Fig. 6 shows adsorption isotherms for Pb, a representative of heavy metals, on the nanocomposite sample and the LTA–goethite mixture. The two isotherms were similar, and both fitted to the Langmuir equation:
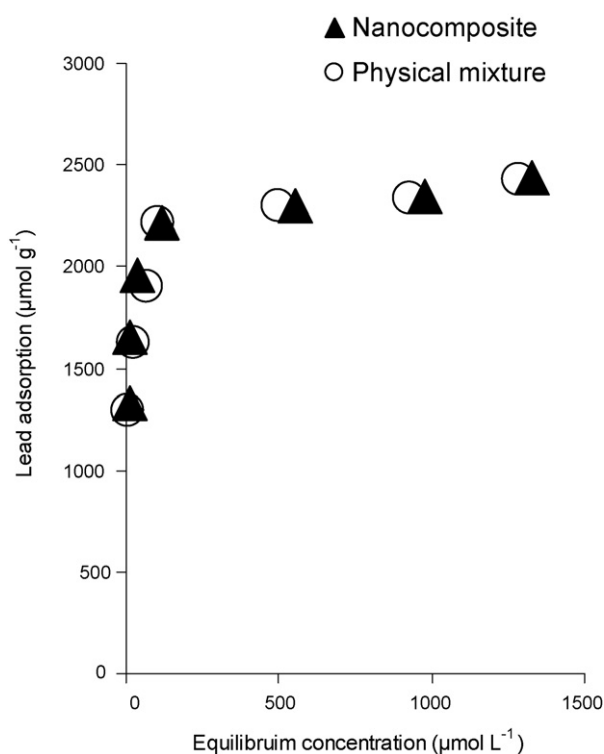
$$\frac{C}{X} = \frac{1}{X_m K} + \frac{C}{X_m}$$

Fig. 6. Pb adsorption isotherms of nanocomposite sample and LTA–goethite mixture. 50 mL of sample was mixed with 30 mL of 0, 2 –5 mM Pb(NO$_3$)$_2$, and shaken at 20 ± 1 °C for 24 h. pH was maintained at 5.00 ± 0.02 throughout the experiment.

where X = amount of adsorption of Pb (μmol g^{-1}), K = a constant related to the binding energy (L μmol^{-1}), X_m = maximum adsorption of Pb (μmol g^{-1}), and C = equilibrium concentration of Pb (μmol L^{-1}). Calculated X_m value was 2500 mmol kg^{-1} for both samples. The K value for the nanocomposite sample (0.077 L μmol^{-1}) was a little bit higher than that for the mixture (0.067 L μmol^{-1}). Similar Pb adsorption property for the nanocomposite sample and the LTA–goethite mixture suggested that synergistic effect was also not generated in the nanocomposite sample in view of Pb adsorptivity.

Fig. 7 shows phosphate adsorption isotherm of the nanocomposite sample, together with isotherms of the LTA–goethite mixture, synthetic LTA and synthetic goethite. Table 1 shows corresponding equilibrium pH values after the phosphate adsorption. Although the adsorption isotherm of the nanocomposite sample did not fit to the Langmuir equation, the adsorption isotherms of the LTA–goethite mixture, synthetic LTA and synthetic goethite fitted well to the Langmuir equation: the Langmuir X_m and K values were 312 μmol g^{-1} and 0.0027 L μmol^{-1} for the LTA–goethite mixture, 105 μmol g^{-1} and 0.0023 L μmol^{-1} for synthetic LTA, and 250 μmol g^{-1} and 0.0022 L μmol^{-1} for synthetic goethite. Both the nanocomposite sample and the LTA–goethite mixture generated

Table 1
Equilibruim pH after phosphate adsorption

Initial concentration (mM)	Nanocomposite	Mixture	LTA	Goethite
0	9.7	9.9	9.8	8.8
1	8.7	8.6	8.6	7.1
2	8.1	7.8	7.8	6.8
3	7.6	7.4	7.4	6.6
4	7.4	7.3	7.3	6.2

50 mg of sample was mixed with 30 mL of 0–4 mM NaH$_2$PO$_4$, and shaken at 20 ± 1 °C for 24 h.
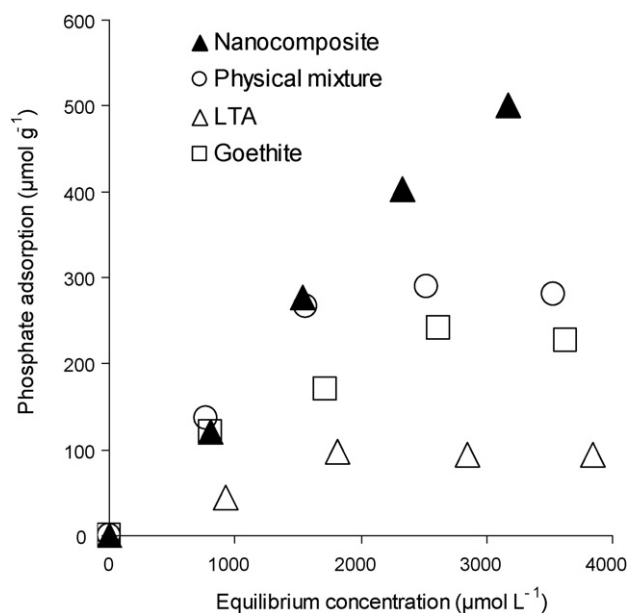

Fig. 7. Phosphate adsorption isotherms of nanocomposite sample, LTA–goethite mixture, synthetic LTA, and synthetic goethite. 50 mg of sample was mixed with 30 mL of 0–4 mM NaH$_2$PO$_4$, and shaken at 20 ± 1 °C for 24 h.

higher phosphate adsorption potential than the synthetic goethite (Fig. 7) and other iron oxides such as magnetite (X_m = 168 μmol g^{-1} at equilibrium pH 3; [24]).

Fig. 7 shows that between phosphate equilibrium concentrations of 0–2 mM, adsorption isotherms of both the nanocomposite sample and the LTA–goethite mixture were the same. However, for phosphate equilibrium concentration of more than 2 mM, the amount of phosphate adsorbed by the nanocomposite sample increased to a maximum of 500 μmol g^{-1} while phosphate adsorption on the LTA–goethite mixture remained relatively constant. From initial phosphate concentration of 2–4 mM, equilibrium pH after phosphate adsorption was concurrently higher for the nanocomposite sample than the LTA–goethite mixture (Table 1). Increase in phosphate adsorption by the nanocomposite sample might not therefore be due to equilibrium pH effect. In view of phosphate adsorption, the increase in adsorption indicates that synergistic effect was much generated in the nanocomposite sample compared to the physically mixed sample at high initial phosphate concentrations. Closer approach between goethite and LTA crystals in the nanocomposite sample, as indicated in Section 3.1, might have caused this synergistic effect. One probable mechanism for the increase in phosphate adsorption is the strong adsorption and binding of phosphate by bridging LTA and goethite crystals.

4. Conclusions

Nanocomposite, consisting of LTA zeolite and goethite was successfully obtained by synthesizing LTA in two steps in the presence of goethite. SEM images revealed closer association between the two crystals as compared to a physically mixed sample. Precipitation of silica on goethite surface and subsequent formation of Si–O–Fe bonds between silica and goethite in the first step contributed to stable LTA–goethite nanocomposite formation. The nanocomposite generated synergistic effects for phosphate adsorption in both amount and strength of adsorption. It is expected that the LTA–goethite nanocomposite has similar synergistic effect for adsorption of other pollutants. In view of cost, the next step is

to synthesize zeolite–goethite nanocomposites from natural and waste materials.

Acknowledgement

References

[1] D. Wu, B. Zhang, C. Li, Z. Zhang, H. Kong, Simultaneous removal of ammonium and phosphate by zeolite synthesized from fly ash as influenced by salt treatment, J. Colloid Inter. Sci. 304 (2006) 300–306.

[2] S. Babel, T.A. Kurniawan, Low-cost adsorbents for heavy metals uptake from contaminated water: a review, J. Hazard. Mater. 97 (2003) 219–243.

[3] T. Henmi, Synthesis of hydroxy-sodalite ("zeolite") from waste coal ash, Soil Sci. Plant Nutr. 33 (1987) 519–523.

[4] H. Ishimoto, M. Yasuda, O. Sasaki, Use of papermaking sludge as new material, J. Mater. Civil Eng. 12 (2000) 310–313.

[5] M. Stachowicz, T. Hiemstra, W.H. van Riemsdijk, Multi–competitive interaction of As (III) and As(V) oxyanions with Ca^{2+}, Mg^{2+}, PO_4^{3-}, and CO_3^{2-} ions on goethite, J. Colloid Inter. Sci. 320 (2008) 400–414.

[6] S. Fukugaichi, A. Uramoto, H. Ichiura, M. Morikawa, S. Kyougoku, K. Nagashima, T. Yamamoto, N. Matsue, T. Henmi, Synthesis of artificial zeolites containing titanium dioxide and their abilities for removing bad smell substances, Jpn. Tappi J. 60 (2006) 1561–1570.

[7] Z.H. Zhou, J.H. Yang, L.F. Chang, Y. Zhang, W.G. Sun, J.Q. Wang, Novel preparation of NaA/carbon nanocomposite thin films with high permeance for CO_2/CH_4 separation, Chin. Chem. Lett. 18 (2007) 455–457.

[8] A. Pourahmad, Sh. Sohrabnezhad, M.S. Sadjadi, K. Zare, Preparation and characterization of host (mesoporous aluminosilicate material)–guest (semiconductor nanoparticles) nanocomposite materials, Mater. Lett. 62 (2008) 655–658.

[9] C. Bisio, C. Caldeira, V. Dal Santo, G. Martra, P. Massiani, R. Psaro, M.F. Ribeiro, J.M. Silva, L. Stievano, Nanocomposite catalytic materials: synthesis, characterization and reactivity of Pt/Cs–BEA zeolites, Inorg. Chim. Acta 349 (2003) 227–238.

[10] Q. Zhai, S. Qiu, F. Xiao, Z. Zhang, C. Shao, Y. Han, Preparation, characterization, and optical properties of the host-guest nanocomposite material zeolite-silver iodide, Mat. Res. Bullet. 35 (2000) 59–73.

[11] D.G. Lewis, U. Schwertmann, The influence of Al on the formation of iron oxide. IV. The influence of [Al], [OH] and temperature, Clays Clay Miner. 27 (1979) 195–200.

[12] U. Schwertmann, H. Thalmann, The influence of Fe(II), Si and pH on the formation of lepidocrocite and ferrihydrite during oxidation of aqueous $FeCl_2$ solutions, Clay Miner. 11 (1976) 189–200.

[13] D.W. Breck, Zeolite Molecular Sieves: Structure, Chemistry, and Use, John Wiley, New York, 1974.

[14] R.W. Thompson, M.J. Huber, Analysis of the growth of molecular sieve zeolite NaA in a batch precipitation system, J. Cryst. Gr. 56 (1982) 711–722.

[15] U. Schwertmann, R.M. Cornell, Iron Oxides in the Laboratory: Preparation and Characterization, VCH, Weinheim, 1991.

[16] J. Murphy, J.P. Riley, A modified single solution method for the determination of phosphate in natural waters, Anal. Chim. Acta 27 (1962) 31–36.

[17] R.W. Thompson, K.C. Franklin, Linde Type A, in: H. Robson (Ed.), Verified Syntheses of Zeolitic Materials, 2nd revised ed., Elsevier Science B.V., Amsterdam, The Netherlands, 2001, pp. 179–180.

[18] Q. Williams, L. Guenther, Pressure-induced changes in the bonding and orientation of hydrogen in FeOOH-goethite, Solid State Commun. 100 (1996) 105–109.

[19] P. Cambier, Infrared study of goethites of varying crystallinity and particle size. I. Interpretation of OH and lattice vibration frequencies, Clay Miner. 21 (1986) 191–200.

[20] R. Raman, B. Kuban, A. Razvan, The application of infrared spectroscopy to the study of atmospheric rust system. 1. Standard spectra and illustrative applications to identify rust phases in natural atmospheric corrosion products, Corros. Sci. 32 (1991) 1295–1306.

[21] D. Scarano, A. Zecchina, S. Bordiga, F. Geobaldo, G. Spoto, G. Petrini, G. Leofanti, M. Padovan, G. Tozzola, Fourier–transform infrared and Raman spectra of pure and Al-, B-, Ti- and Fe-substituted silicalites: stretching-mode region, J. Chem. Soc., Faraday Trans. 89 (1993) 4123–4130.

[22] Y. Xu, L. Axe, Synthesis and characterization of iron oxide-coated silica and its effect on metal adsorption, J. Colloid Inter. Sci. 282 (2005) 11–19.

[23] E. Doelsch, A. Masion, J. Rose, W.E.E. Stone, J.Y. Bottero, P.M. Bertsch, Chemistry and structure of colloids obtained by hydrolysis of Fe(III) in the presence of SiO_4 ligands, Colloids Surf. A: Physicochem. Eng. Aspects 217 (2003) 121–128.

[24] T.J. Daou, S. Begin-Colin, J.M. Grenéche, F. Thomas, A. Derory, P. Bernhardt, P. Legaré, G. Pourroy, Phosphate adsorption properties of magnetite-based nanoparticles, Chem. Mater. 19 (2007) 4494–4505.